Enhanced resolution in subsurface near-field optical microscopy

Roman Krutokhvostov,[1] **Alexander A. Govyadinov,**[1]
Johannes M. Stiegler,[1] **Florian Huth,**[1,2] **Andrey Chuvilin,**[1,3]
P. Scott Carney,[1,4] **and Rainer Hillenbrand**[1,3,*]

[1]*CIC nanoGUNE Consolider, E-20018, Donostia-San Sebastián, Spain*
[2]*Neaspec GmbH, D-82152, Martinsried, Germany*
[3]*IKERBASQUE, Basque Foundation for Science, E-48011 Bilbao, Spain*
[4]*ECE Dept. and Beckman Institute, University of Illinois at
Urbana-Champaign, Urbana, IL 61801, USA*

[*]*r.hillenbrand@nanogune.eu*

Abstract: We report an experimental analysis of the capabilities of scattering-type scanning near-field optical microscopy for mapping subsurface features at varying depths. For the first time, we demonstrate experimentally that both the spatial resolution and depth contrast can be improved in subsurface microscopy by demodulating the measured near-field signal at higher harmonics of the probe's tapping frequency and by operating at smaller tapping amplitudes. Our findings are qualitatively supported by a simple dipole model.

© 2011 Optical Society of America

OCIS codes: (180.4243) Near-field microscopy; (110.3080) Infrared imaging.

References and links

1. B. Knoll and F. Keilmann, "Near-field probing of vibrational absorption for chemical microscopy," Nature **399**, 134–137 (1999).
2. B. B. Akhremitchev, S. Pollack, and G. C. Walker, "Apertureless scanning near-field infrared microscopy of a rough polymeric surface," Langmuir **17**, 2774–2781 (2001).
3. R. Hillenbrand and F. Keilmann, "Material-specific mapping of metalsemiconductordielectric nanosystems at 10 nm resolution by backscattering near-field optical microscopy," Appl. Phys. Lett. **80**, 25–27 (2002).
4. Z. H. Kim, S.-H. Ahn, B. Liu, and S. R. Leone, "Nanometer-scale dielectric imaging of semiconductor nanoparticles: size-dependent dipolar coupling and contrast reversal," Nano Lett. **7**, 2258–2262 (2007).
5. A. J. Huber, F. Keilmann, J. Wittborn, J. Aizpurua, and R. Hillenbrand, "Terahertz near-field nanoscopy of mobile carriers in single semiconductor nanodevices," Nano Lett. **8**, 3766–3770 (2008).
6. J. M. Stiegler, A. J. Huber, S. L. Diedenhofen, J. Gómez Rivas, R. E. Algra, E. P. A. M. Bakkers, and R. Hillenbrand, "Nanoscale free-carrier profiling of individual semiconductor nanowires by infrared near-field nanoscopy," Nano Lett. **10**, 1387–1392 (2010).
7. F. Huth, M. Schnell, J. Wittborn, N. Ocelic, and R. Hillenbrand, "Infrared-spectroscopic nanoimaging with a thermal source," Nat Mater **10**, 352–356 (2011).
8. M. B. Raschke and C. Lienau, "Apertureless near-field optical microscopy: Tip–sample coupling in elastic light scattering," Appl. Phys. Lett. **83**, 5089–5091 (2003).
9. T. Taubner, F. Keilmann, and R. Hillenbrand, "Nanoscale-resolved subsurface imaging by scattering-type near-field optical microscopy," Opt. Express **13**, 8893–8899 (2005).
10. T. Taubner, D. Korobkin, Y. Urzhumov, G. Shvets, and R. Hillenbrand, "Near-field microscopy through a sic superlens," Science **313**, 1595 (2006).
11. J.-S. Samson, G. Wollny, E. Brundermann, A. Bergner, A. Hecker, G. Schwaab, A. D. Wieck, and M. Havenith, "Setup of a scanning near field infrared microscope (snim): Imaging of sub-surface nano-structures in gallium-doped silicon," Phys. Chem. Chem. Phys. **8**, 753–758 (2006).
12. G. Wollny, E. Bründermann, Z. Arsov, L. Quaroni, and M. Havenith, "Nanoscale depth resolution in scanning near-field infrared microscopy," Opt. Express **16**, 7453–7459 (2008).

13. J. Sun, J. Schotland, R. Hillenbrand, and P. S. Carney, "Nanoscale optical tomography using volume-scanning near-field microscopy," Appl. Phys. Lett. **95**, 121108 (2009).
14. R. Jacob, S. Winnerl, H. Schneider, M. Helm, M. T. Wenzel, H.-G. von Ribbeck, L. M. Eng, and S. C. Kehr, "Quantitative determination of the charge carrier concentration of ion implanted silicon by ir-near-field spectroscopy," Opt. Express **18**, 26206–26213 (2010).
15. R. Hillenbrand and F. Keilmann, "Near-field microscopy by elastic light scattering from a tip," Phil. Trans. R. Soc. Lond. A **362**, 787–805 (2004).
16. L. Novotny and B. Hecht, *Principles of Nano-Optics* (Cambridge University Press, 2006).
17. R. Hillenbrand and F. Keilmann, "Complex optical constants on a subwavelength scale," Phys. Rev. Lett. **85**, 3029–3032 (2000).
18. T. Taubner, F. Keilmann, and R. Hillenbrand, "Effect of tip modulation on image contrast in scattering-type near-field optical microscopy," J. Kor. Phys. Soc. **47**, S213–S216 (2005).
19. Z. Nuño, B. Hessler, J. Ochoa, Y.-S. Shon, C. Bonney, and Y. Abate, "Nanoscale subsurface- and material-specific identification of single nanoparticles," Opt. Express **19**, 20865–20875 (2011).
20. N. Ocelic, A. Huber, and R. Hillenbrand, "Pseudoheterodyne detection for background-free near-field spectroscopy," Appl. Phys. Lett. **89**, 101124 (2006).
21. T. Taubner, R. Hillenbrand, and F. Keilmann, "Performance of visible and mid-infrared scattering-type near-field optical microscopes," J. Microscopy **210**, 311–314 (2003).
22. E. Betzig and J. K. Trautman, "Near-field optics: Microscopy, spectroscopy, and surface modification beyond the diffraction limit," Science **257**, 189–195 (1992).
23. R. Esteban, R. Vogelgesang, and K. Kern, "Full simulations of the apertureless scanning near field optical microscopy signal: achievable resolution and contrast," Opt. Express **17**, 2518–2529 (2009).
24. V. A. Markel, "Coupled-dipole approach to scattering of light from a one-dimensional periodic dipole chain," J. Mod. Opt. **40**, 2281–2291 (1993).
25. F. Zenhausern, Y. Martin, and H. K. Wickramasinghe, "Scanning interferometric apertureless microscopy: Optical imaging at 10 angstrom resolution," Science **269**, 1083–1085 (1995).
26. B. Knoll and F. Keilmann, "Enhanced dielectric contrast in scattering-type scanning near-field optical microscopy," Opt. Comm. **182**, 321–328 (2000).
27. B. Knoll and F. Keilmann, "Infrared conductivity mapping for nanoelectronics," Appl. Phys. Lett. **77**, 3980–3982 (2000).
28. R. Hillenbrand, T. Taubner, and F. Keilmann, "Phonon-enhanced light matter interaction at the nanometre scale," Nature **418**, 159–162 (2002).
29. A. Cvitkovic, N. Ocelic, J. Aizpurua, R. Guckenberger, and R. Hillenbrand, "Infrared imaging of single nanoparticles via strong field enhancement in a scanning nanogap," Phys. Rev. Lett. **97**, 060801 (2006).
30. A. Cvitkovic, N. Ocelic, and R. Hillenbrand, "Material-specific infrared recognition of single sub-10 nm particles by substrate-enhanced scattering-type near-field microscopy," Nano Lett. **7**, 3177–3181 (2007).
31. A. Cvitkovic, N. Ocelic, and R. Hillenbrand, "Analytical model for quantitative prediction of material contrasts in scattering-type near-field optical microscopy," Opt. Express **15**, 8550–8565 (2007).
32. J. M. Stiegler, Y. Abate, A. Cvitkovic, Y. E. Romanyuk, A. J. Huber, S. R. Leone, and R. Hillenbrand, "Nanoscale infrared absorption spectroscopy of individual nanoparticles enabled by scattering-type near-field microscopy," ACS Nano **5**, 6494–6499 (2011).

Scattering-type scanning near-field optical microscopy (s-SNOM) is a versatile scanning probe technique for nondestructive optical imaging with nanometer-scale spatial resolution. In particular, it enables spectroscopic nano-imaging of local chemical composition, free-carrier concentration in semiconducting nanostructures and molecular vibrational contrast of organic samples [1–7]. It has recently been shown that in addition to examining the sample exterior, s-SNOM is also sensitive to features buried below the surface [6, 8–14].

At early stages, s-SNOM suffered from parasitic scattering (background) caused by the sample roughness or microscope tip shaft. The background can be efficiently suppressed by operating the microscope in the tapping regime, in which the probe is oscillated sinusoidally and the resulting signal is demodulated at higher harmonics of the oscillation frequency [15–17]. It has also been shown that the near-field *material contrast* (the ratio between the complex-valued near-field signals from different materials) at the sample surface [17, 18] and slightly below it [19] can be enhanced by higher harmonic demodulation or by decreasing the tapping amplitude of the probe. However, no systematic study of the influence of these parameters on the spatial resolution and depth contrast in subsurface s-SNOM has been performed so far. In this
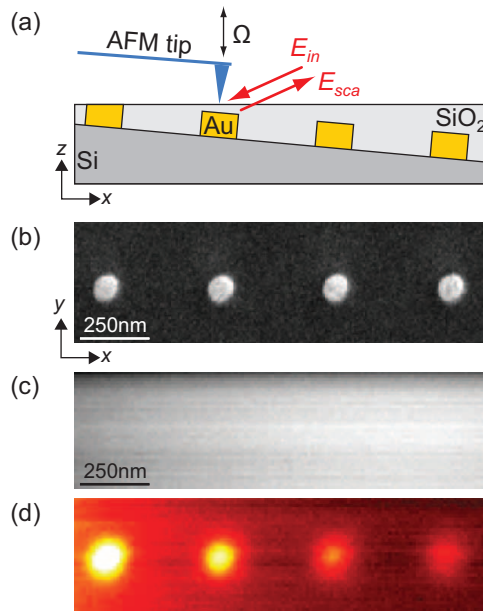
Fig. 1. Subsurface infrared near-field imaging. (a) Experimental set-up and sketch of the cross-section of the sample, containing 100 nm diameter Au disks covered by SiO_2. (b) SEM image of the Au disks before SiO_2 deposition. (c) AFM topography of the SiO_2 surface. (d) Image of the infrared near-field amplitude s_3 at $A = 70$ nm recorded simultaneously with topography.

work we demonstrate, for the first time, that the near-field *depth contrast* (the contrast between equal objects located at different depths), as well as the *spatial resolution* in subsurface imaging can be improved by operating at smaller tapping amplitudes and/or by recording higher temporal harmonics of the near-field signal.

s-SNOM is typically based on an atomic force microscope (AFM), where a sharp metallic probe tip is illuminated by a focused laser beam of wavelength λ. Besides probing the surface topography, the AFM tip functions as an optical antenna converting the illuminating radiation into a highly localized and enhanced near field at the tip apex [15, 16]. Due to the optical near-field interaction between the tip and the sample, the scattered radiation is modified in both its amplitude and phase, depending on the local dielectric properties of the sample. By interferometric detection of the backscattered light it is possible to record amplitude and phase images, which contain information about the local complex-valued dielectric properties of the sample. Besides the desired near-field signal, these images contain a large amount of background, caused by scattering at the AFM cantilever, tip shaft, etc. In tapping regime, the distance between the tip and the sample is modulated periodically by driving the tip to oscillate vertically at a tapping frequency Ω and amplitude A ($A \ll \lambda$). The subsequent demodulation of the detected optical signal at higher harmonics $n\Omega$ with $n > 2$ yields, essentially, background-free nanoscale-resolved near-field optical amplitude s_n and phase φ_n images [15–17].

Below we experimentally explore the influence of the parameters A and n on the ability of s-SNOM to detect and resolve nanostructures *buried below the sample surface*. We demonstrate that, despite weaker signals, tapping with small amplitudes and detection at higher harmonics n result in an enhancement of the resolving power of the microscope.

Our experimental set-up, based on NeaSNOM from Neaspec, is schematically depicted in

Fig. 1(a). A metallized AFM tip (apex radius: $R \simeq 20$ nm), oscillating at its resonant frequency ($\Omega \simeq 250$ KHz) is illuminated by infrared (IR) light (E_{in}) from a CO_2-laser ($\lambda = 11.31$ μm). The backscattered light (E_{sca}) is collected with a parabolic mirror and analyzed with a pseudo-heterodyne Michelson interferometer. Demodulation of the interferometer signal at higher harmonics n yields amplitude and phase signals s_n and φ_n, respectively [20]. In order to study the influence of the tapping amplitude A and the demodulation order n on resolution and depth contrast, we recorded near-field amplitude images of a test sample with subsurface nanostructures at two different tapping amplitudes $A = 20$ nm and $A = 70$ nm, while the signal demodulation was done at the third ($n = 3$) and fourth ($n = 4$) harmonics of the tapping frequency.

Our test sample consists of a sequence of subsurface gold disks with diameters of 100 nm, a height of 40 nm and a center-to-center separation of 400 nm. The disks were fabricated by focused ion beam (FIB) milling of a Au film, which was sputtered on a Si wafer. The choice of Au and Si was motivated by their well-defined near-field infrared contrast [17,21]. The Au disks shown in Fig. 1(b) were coated with a SiO_2 layer, which was polished with FIB at a small angle of about 2°. This way, a well-known test sample (Fig. 1(a)) with linearly increasing thickness of the capping SiO_2 layer and a smooth surface was manufactured. We note that the Au disks are non-resonant at infrared frequencies at which the near-field measurements are performed (neither is the tip).

The topography image (Fig. 1(c)) of the test sample confirms that the surface of the SiO_2 is flat and homogeneously polished, while the IR near-field image (Fig. 1(d)) clearly reveals the gold disks below the SiO_2 surface. We observe a decrease of the IR amplitude signal and blurring of the IR near-field pattern of the gold disks due to the rapid decay of the near-field signal with increasing thickness of the SiO_2 layer.
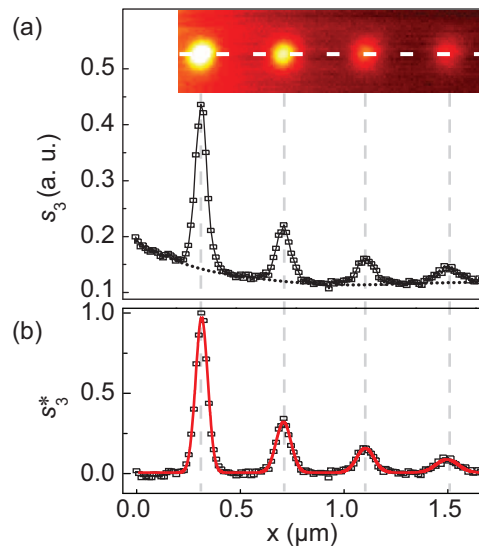

Fig. 2. (a) Near-field amplitude profile s_3 recorded at $A = 70$ nm, extracted from the IR near-field image (inset) along the dashed white line. Symbols represent experimental data, the black solid line – a linear interpolation between the data points and black dots – a baseline. (b) Baseline-corrected, normalized amplitude s_3^*. Symbols represent the experimental data and the red solid line shows a Gaussian fit.

Figure 2(a) shows a profile of near-field amplitude s_3 at $A = 70$ nm (black solid line in panel (a)), extracted along the centers of the disks (dashed line in the inset). A series of peaks, cor-

responding to the gold disks, is seen on top of a baseline signal (dotted line in Fig. 2(a)). The baseline signal can be attributed to the near-field interaction between the tip and the Si substrate. We find that both the peak and baseline amplitude signals decrease with x, i.e. when the thickness of the SiO_2 layer increases. This can be explained by the increasing distance between, the tip and the gold disks, and respectively, between the tip and the Si surface, which reduces the near-field interaction and thus the field scattered from the tip. In order to analyze quantitatively the near-field contrast of the gold disks, we subtracted the baseline and normalized the result to the height of the first peak. For that purpose we measured the near-field profile of s_3 on either sides of the disks, yielding an averaged baseline. We find that the normalized profile s_3^* (Fig. 2(b), symbols) can be well described by Gaussian fits (red solid line), from which the maximum values and the full widths at half maximum (FWHMs) of the peaks can be determined. The FWHMs provide a measure for comparing the apparent widths of the disks and can be used to estimate the lateral resolution in the near-field images. Thus, the increase in FWHMs of the consecutive peaks observed in Fig. 2 reveals the degrading spatial resolution when the distance between the tip and gold disks increases, which is a fundamental characteristic of the near-field microscopy [16, 22].
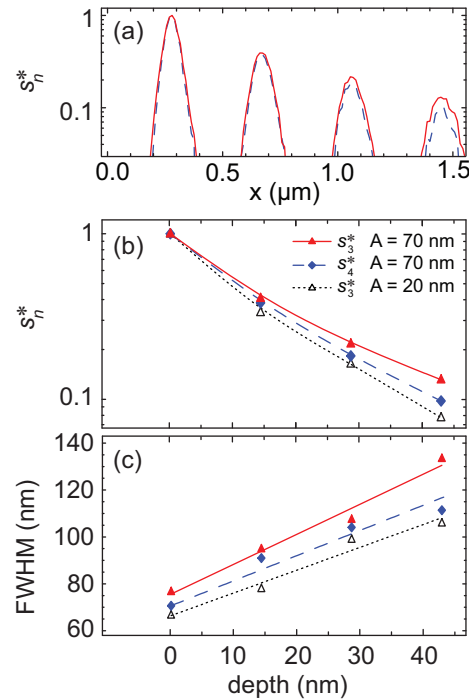

Fig. 3. Comparison of s-SNOM resolution and depth contrast for different imaging parameters A and n. (a) Profiles of near-field amplitudes s_3^* (solid red) and s_4^* (dashed blue) recorded along the white dashed line in Fig. 2(a). Tapping amplitude $A = 70$ nm. (b) Peak maxima obtained from Gaussian fits. (c) FWHMs obtained from Gaussian fits.

We further employed Gaussian fitting in order to compare near-field profiles s_n^* of the disks recorded at different tapping amplitudes A and demodulation orders n. Figure 3(a) shows the near-field amplitude profiles s_3^* and s_4^* at the fixed tapping amplitude of $A = 70$ nm. We observe that the near-field contrast between disks in different depths (*depth contrast*) is enhanced at higher harmonics. Indeed, in Fig. 3(b) we see that the peak maxima of s_4^* decay faster with

increasing depth than the peak maxima of s_3^*. We furthermore find that the FWHMs in the s_4^* profile are smaller than those of the s_3^* profile (Fig. 3(c)), demonstrating the improved spatial resolution in subsurface s-SNOM by higher harmonic signal demodulation. The enhancements of both the resolution and depth contrast at higher harmonics can be attributed to the faster decay of the higher-harmonic near-field amplitudes when the tip-sample distance is increased [8, 18, 21, 23].

The resolution and depth contrast can be also improved by decreasing the tapping amplitude. This can be seen in Figs. 3(b,c) by comparing the FWHMs and the peak values of the s_3^* profile recorded at $A = 20$ nm (black open triangles) with those of the s_3^* profile recorded at $A = 70$ nm (red triangles).

The enhancement of depth contrast at small amplitudes is a direct consequence of the steeper decay of the corresponding approach curves [18]. To understand the enhancement of the resolution at smaller tapping amplitudes one can imagine the following thought experiment. Suppose that one could measure a pure near-field signal from a single gold disk buried in the silicon oxide without vertical tip oscillation and tapping. By scanning the tip horizontally at a *fixed height* above the capping silicon oxide surface, one could obtain the (non-demodulated) near-field image of the disk buried below the surface. With the increase of the tip height, the disk image would blur because of the degrading spatial resolution [22]. Thus, the FWHM of the disk increases as one scans the tip higher above the silicon oxide surface. The demodulation process (that is applied when the tip oscillates vertically) can be thoughts of as a (weighted) average of the disk images taken at different heights. Smaller amplitudes correspond to the averaging over lower tip positions and therefore yield smaller FWHMs of disk images when the demodulation is applied.
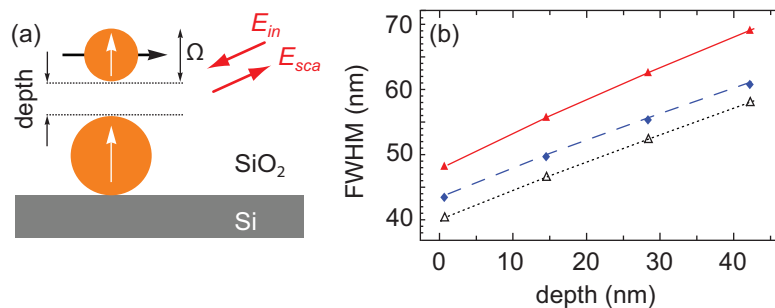

Fig. 4. Qualitative modeling of subsurface s-SNOM. (a) Schematics of the model where the tip and the disk are described by dipoles. (b) Calculated FWHMs for different imaging parameters A and n.

To *qualitatively* confirm the experimentally observed trends, we use a simple model based on the coupled dipole method (CDM) [24]. Here, both the disks and the tip are treated as point dipoles embedded into a SiO_2 host above a Si substrate (Fig. 4(a)). The presence of the SiO_2-air interface was ignored due to smaller refractive index of the SiO_2 compared to that of silicon substrate. The tip dipole is assigned the polarizability of a small sphere with a radius $R = 20$ nm (radius of the tip apex). Each disk dipole is described by the polarizability of a sphere with volume equal to that of the disk (radius of about 42 nm). This model yields an algebraic system of coupled equations for the dipole polarizations [24], from which the scattered field can be calculated. By vertically oscillating the tip sinusoidally, we obtain the scattered field as a function of time, $E_{sca}(t)$. The subsequent Fourier analysis yields the higher harmonic amplitudes s_n. By scanning the tip dipole horizontally across the disk dipoles (indicated by the horizontal

arrow in Fig 4(a)), we obtain calculated line profiles, similar to the experimental ones shown in Fig. 2(b) and Fig. 3(a). From the calculated profiles we determine the FWHMs of the gold disks. The results of our simulations are summarized in Fig. 4(b). We find that the FWHMs of the peaks are reduced at smaller tapping amplitudes and higher harmonics, therefore *confirming the trends* obtained in the experiment.

We note that the CDM model is widely used to verify overall trends in s-SNOM experiments, providing *qualitatively correct* results [1,19,25–30] Quantitative differences between the model and our experiment we attribute to the finite sizes of the tip and the disks, which are not taken into account in the model. In particular, the near-field probe employed in the experiment is a large (several micrometers long) metallized tip. The polarization developed in such tip under the external illumination and due to the near-field interaction with the sample can differ significantly from that of the small sphere representing the tip in the model. Although, a quantitative treatment of s-SNOM contrasts is possible with the finite-dipole model, where the tip is treated as a spheroid [31], this model is only applicable in the case of homogeneous samples [31] or for small spherical nanoparticles located directly below the tip [32]. For describing subsurface near-field contrasts in more complex samples, such as the ones studied in this work, future improved models have to be developed.
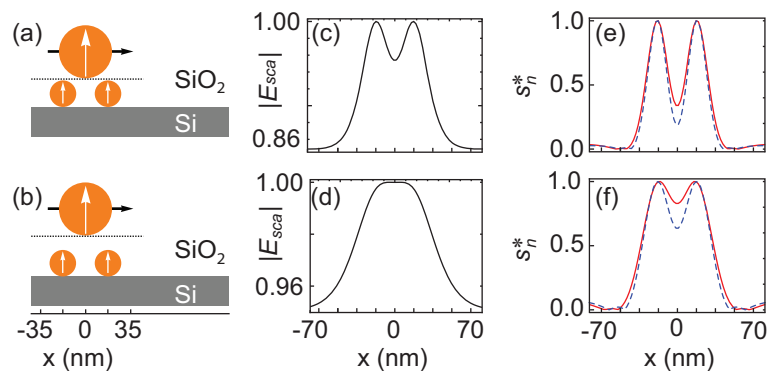

Fig. 5. CDM simulations. (a, b) Schematics of the simulation showing the probe sphere (tip, radius 20 nm) scanning across two small spheres (radii 10 nm). (c, d) Calculated near-field profile E_{sca}. (e, f) Calculated near-field profiles of 3rd (solid red line) and 4th (dashed blue line) harmonics. The top panels show the simulation with the spheres buried right below the SiO_2 surface. The bottom panels show the simulation with the spheres buried at the depth of 15 nm beneath it. All signals are normalized to their own maxima.

We have further utilized the CDM model to simulate the near-field signal E_{sca} and its harmonics s_n as the tip, described as a sphere dipole of 20 nm in radius, scans along a sample consisting of a pair of small Au nano-spheres buried below the SiO_2 surface (Fig. 5). The small spheres are 10 nm in radius and separated by a gap of 15 nm. When the spheres are located right below the tip (a), they can be resolved in the E_{sca} profile (c) and in s_n (e). The situation changes dramatically when the spheres are buried at 15 nm depth (b). The near-field signal E_{sca} exhibits a single peak not revealing the presence of two spheres (d). In contrast, the higher harmonic profiles s_3^* and s_4^* clearly resolve the two spheres (f), which provides a further theoretical support for the enhancement of the resolution by higher harmonic demodulation.

In conclusion, we have demonstrated that the spatial resolution and depth contrast in subsurface s-SNOM can be enhanced by operating at small tapping amplitudes and by demodulating the detector signal at higher harmonics of the tapping frequency. This improvement comes at

the cost of signal strength. Our simulations qualitatively corroborate these experimental findings and indicate that the resolution improvement becomes more significant when smaller, more closely spaced subsurface objects are imaged.

Acknowledgments